Magnetic ordering in multiferroic $SmMn_2O_5$ and $GdMn_2O_5$ studied by resonant soft x-ray scattering

Y. Ishii,[1,*] S. Horio,[1] H. Yamamoto,[1,2] Y. Noda,[2,3] H. Nakao,[3] Y. Murakami,[3] and H. Kimura[1,2]

[1]*Department of Physics, Tohoku University, Aoba, Sendai 980-8578, Japan*

[2]*Institute of Multidisciplinary Research for Advanced Materials, Tohoku University, Aoba Sendai 980-8577, Japan*

[3]*Condensed Matter Research Center and Photon Factory, Institute of Materials Structure Science (IMSS), High Energy Accelerator Research Organization (KEK), Tsukuba, Ibaraki 305-0801, Japan*

(Received 2 August 2018; revised manuscript received 26 September 2018; published 21 November 2018)

Resonant soft x-ray scattering was used to study the magnetic ordering of the multiferroic materials $SmMn_2O_5$ and $GdMn_2O_5$. In the case of $SmMn_2O_5$, the results confirm that antiferromagnetic ordering of Mn magnetic moments occurs with magnetic propagation vector $\mathbf{q}_M = (1/2, 0, 1/3 + \delta')$ in the incommensurate magnetic phase, followed by the appearance of the commensurate magnetic phase with $\mathbf{q}_M = (1/2, 0, 0)$ as the temperature is decreased. The energy spectrum around Mn $L_{II,III}$ edges suggests that the Mn ions adopt unique electronic states in the CM phase of $SmMn_2O_5$. No evidence was found for spin polarization of oxygen ions through $2p$-$3d$ orbital hybridization between oxygen and Mn ions in this compound, although this phenomenon is clearly evident in $GdMn_2O_5$ and other RMn_2O_5 (R = Y, Er, Tb) compounds. The energy spectra around O K edge strongly suggest that electronic polarization resulting from charge transfer between oxygen and Mn ions has little contribution to the ferroelectricity while lattice distortion likely plays a key role in promoting ferroelectricity in $SmMn_2O_5$.

DOI: 10.1103/PhysRevB.98.174428

I. INTRODUCTION

Multiferroic materials exhibiting two or more ferroic order parameters that coexist and couple strongly with one another have attracted a great deal of attention for several decades. Among these materials, so-called type II multiferroics [1], in which ferroelectricity is driven by magnetic ordering, exhibit interesting phenomena such as nonlinear gigantic magnetoelectric (ME) effects.

Multiferroic RMn_2O_5 (R = rare-earth) compounds show various ME effects, such as flipping and flopping of the electric polarization in response to the application of a magnetic field in $TbMn_2O_5$ and $TmMn_2O_5$, respectively [2,3]. Many experimental studies for RMn_2O_5 materials including neutron and x-ray scattering have proposed that complex magnetic ordering of Mn^{4+} and Mn^{3+} ions induces electric polarization as a result of the break of inversion symmetry via exchange and Dzyaloshinskii-Moriya interactions, which are proportional to the scalar product ($\mathbf{S}_i \cdot \mathbf{S}_j$) and the vector product ($\mathbf{S}_i \times \mathbf{S}_j$) of neighboring spins, respectively [3–7]. It has been revealed that nonlinear ME effects in RMn_2O_5 compounds are caused by simultaneous complex dielectric and magnetic phase transitions induced by external field such as temperature variations and magnetic fields [8–11].

On the more microscopic scale, there are two electric polarization mechanisms; ionic and electronic polarization (referred to herein as $\mathbf{P}_{ion}$ and $\mathbf{P}_{ele}$, respectively). These effects are cased by magnetically driven distortions of an ionic lattice and charge transfer through orbital hybridization between ions, respectively. Some theoretical and experimental investigations have pointed out that the both $\mathbf{P}_{ion}$ and $\mathbf{P}_{ele}$ could contribute to electric polarization in RMn_2O_5 [12–14]. Furthermore recent resonant soft x-ray scattering (RSXS) experiment around O K edge for YMn_2O_5 has provided evidence that spin polarization of oxygen ions occurs through charge transfer between oxygen and Mn ions with the $2p$-$3d$ orbital hybridization [15]. It has been concluded that $\mathbf{P}_{ele}$ plays a major role for the ferroelectricity, based on the one-to-one correspondence between temperature dependence of resonant scattering intensity at O K edge and that of the electric polarization. The spin polarization of oxygen ions via p-d hybridization has also been observed in other RMn_2O_5 (R = Tb, Er) and $RMnO_3$ (R = Tb, Dy) compounds [16–18].

In the case of $SmMn_2O_5$, the microscopic magnetic properties had not been examined due to a large neutron absorption cross section of the Sm ions in this compound. Recently, our group carried out resonant hard x-ray scattering (RHXS) experiments to investigate the magnetic ordering of Sm and Mn ions, and determined the dielectric and magnetic phase diagram [19]. The Sm and Mn magnetic moments are aligned with $\mathbf{q}_M = (1/2 + \delta, 0, 0)$ below T_{N3} ($=T_{C2}$) $\simeq$ 28 K, which coincide with the large electric polarization [see Fig. 5 of Ref. [19] as well as Fig. 6(d) shown later] in this material compared with that of other RMn_2O_5 compounds. The ordering of both Sm and Mn moments change to commensurate order with $\mathbf{q}_M = (1/2, 0, 0)$ at $T_{CM} \simeq 26$ K. Therefore we identified these phases as ICM2 and CM phases as shown in Fig. 1. We found that the Sm and Mn ions had an almost collinear magnetic structure in the CM phase, in which the magnetic moments were oriented in the direction to the c axis. In addition, measurements of dielectric properties and

*yuta.ishii.s4@dc.tohoku.ac.jp

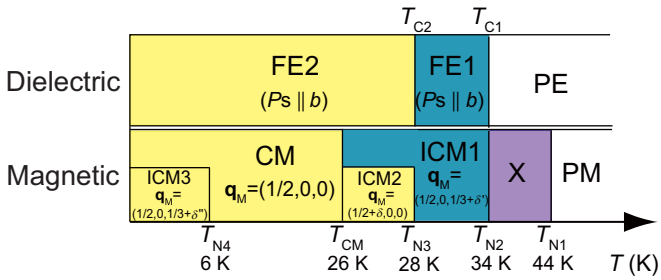

FIG. 1. Dielectric and magnetic phase diagrams of $SmMn_2O_5$. The abbreviations have the following meanings: PE: paraelectric, FE1: ferroelectric 1, FE2: ferroelectric 2, PM: Paramagnetic, ICM1: incommensurate magnetic 1, ICM2: incommensurate magnetic 2, CM: commensurate magnetic, ICM3: incommensurate magnetic 3. The ICM1 and ICM3 phases were reported in Ref. [19]. The phase transition temperatures were determined to be $T_{N1} \simeq 44$ K, T_{N2} ($= T_{C1}$) $\simeq 34$ K, T_{N3} ($= T_{C2}$) $\simeq 28$ K, $T_{CM} \simeq 26$ K, and $T_{N4} \simeq 6$ K.

magnetic susceptibilities indicated another ferroelectric and magnetic phase transitions at $T_{N1} \simeq 44$ K, T_{N2} ($=T_{C1}$) $\simeq$ 34 K, and $T_{N4} \simeq 6$ K [19]. Quite recently, powder neutron scattering experiments for $SmMn_2O_5$ containing the ^{154}Sm isotope were performed by Yahia *et al.* [20]. This prior work showed that the Mn ions in this compound align with $\mathbf{q}_M = (1/2, 0, 1/3+\delta')$ in the range of $T_{CM} < T < T_{N2}$, and that another incommensurate magnetic ordering with $\mathbf{q}_M = (1/2, 0, 1/3+\delta'')$ appears below $T = T_{N4}$ and coexists with the CM phase. Figure 1 represents these phases as ICM1 and ICM3 phases, respectively. Yahia *et al.* also determined the magnetic structure in the CM phase of $SmMn_2O_5$, which was almost equivalent to that previously reported by our own group [19]. However, it is still not clear whether or not spin polarization of oxygen ions occurs in $SmMn_2O_5$. In addition, the microscopic origin of the large electric polarization in the CM phase is also not yet known.

In the present study, we employed resonant soft x-ray scattering (RSXS) to observe the magnetic ordering of Sm, Mn, and oxygen ions. The energy spectrum around O *K* edge shows a lack of well-defined peaks from the $2p$-$3d$ hybridization between oxygen and Mn ions, which strongly suggests that $\mathbf{P}_{ele}$ makes no appreciable contribution to the large electric polarization in the CM phase of $SmMn_2O_5$. We also applied RSXS to the analysis $GdMn_2O_5$ and compared the spectra with those obtained from $SmMn_2O_5$.

II. EXPERIMENTAL DETAILS

Single crystals of $SmMn_2O_5$ and $GdMn_2O_5$ were grown using the PbO-PbF_2 flux method [21]. For the RSXS experiments, samples of $SmMn_2O_5$ with (1, 0, 0)- and (3, 0, 2)-surface normal, and $GdMn_2O_5$ with (1, 0, 0)-surface normal were prepared.

RSXS experiments were performed around Sm M_{IV} ($E \sim$ 1089 eV), Mn $L_{II,III}$ ($E \sim 653$ eV, 645 eV, respectively), and O *K* ($E \sim 530$ eV) edges for $SmMn_2O_5$, which correspond to Sm $3d \Leftrightarrow 4f$, Mn $2p \Leftrightarrow 3d$, and O $1s \Leftrightarrow 2p$ dipole transitions, respectively. RSXS experiment were also carried out around the Mn $L_{II,III}$ and O *K* edges for $GdMn_2O_5$. We used the silicon drift detector, an energy resolution of

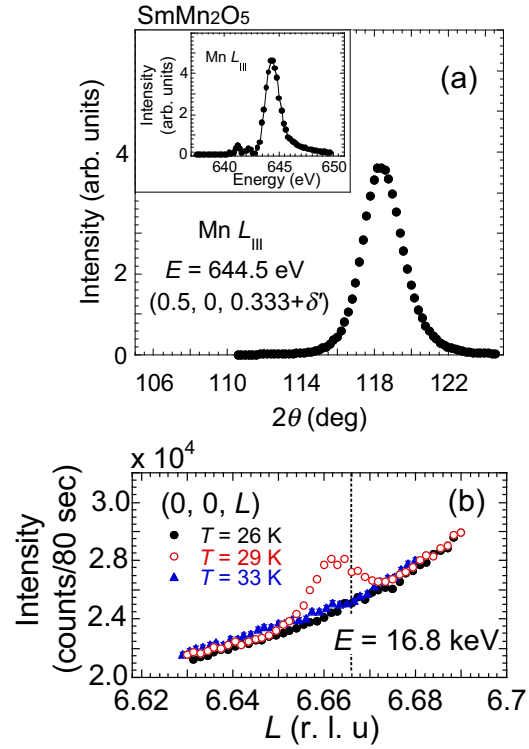

FIG. 2. (a) Peak profile obtained from θ-2θ scans around $\mathbf{Q} = (0.5, 0, 0.333+\delta')$ at $T = 31$ K and at Mn L_{III} $E = 644.5$ eV for $SmMn_2O_5$. The inset shows energy spectrum around Mn L_{III} edge at $\mathbf{Q} = (0.5, 0, 0.333+\delta')$ at $T = 31$ K. (b) Lattice modulation reflections around $\mathbf{Q} = (0, 0, 6.66)$ at $T = 26$ K (filled circles), $T = 29$ K (open circles), and $T = 33$ K (filled triangles). The dashed line indicates $L = 6.666$.

which is less than 100 eV, to exclude higher-order harmonics such as $\lambda/2$ scattering. In addition, the lattice modulation of $SmMn_2O_5$ was observed by hard x-ray diffraction at $E =$ 16.8 keV. RSXS and lattice modulation measurements were performed at the BL-19B, BL-16A [22], and BL-4C at the Photon Factory in the High Energy Accelerator Research Organization (KEK), Japan.

III. RESULTS

Figure 2(a) presents the results of a θ-2θ scans around momentum transfer $\mathbf{Q} = (0.5, 0, 0.333+\delta')$ at Mn L_{III} edge and at $T = 31$ K for $SmMn_2O_5$. The incident x-ray was π polarized. Energy spectrum around Mn L_{III} edge is also provided in the inset to Fig. 2(a). A well-defined peak was observed at Mn L_{III} edge only between $T_{CM} \sim 26$ K and $T_{N2} \sim 34$ K. The δ' value varies with temperature. These observations confirm that the Mn moments aligned antiferromagnetically with $\mathbf{q}_M = (1/2, 0, 1/3+\delta')$ in the ICM1 phase ($T_{CM} < T < T_{N2}$), which is consistent with previously reported results [20]. As shown in Fig. 2(b), a superlattice reflection at $\mathbf{Q} = (0, 0, 6.666 + 2\delta')$ was observed at $T = 29$ K, which appeared between T_{N3} and T_{N2}. The position of this reflection corresponds to lattice modulation with $\mathbf{q}_L = (0, 0, 2/3 + 2\delta')$. Studies of RMn_2O_5 compounds have shown that the $\mathbf{q}_M$ value for these compounds is exactly half the $\mathbf{q}_L$ value, meaning that

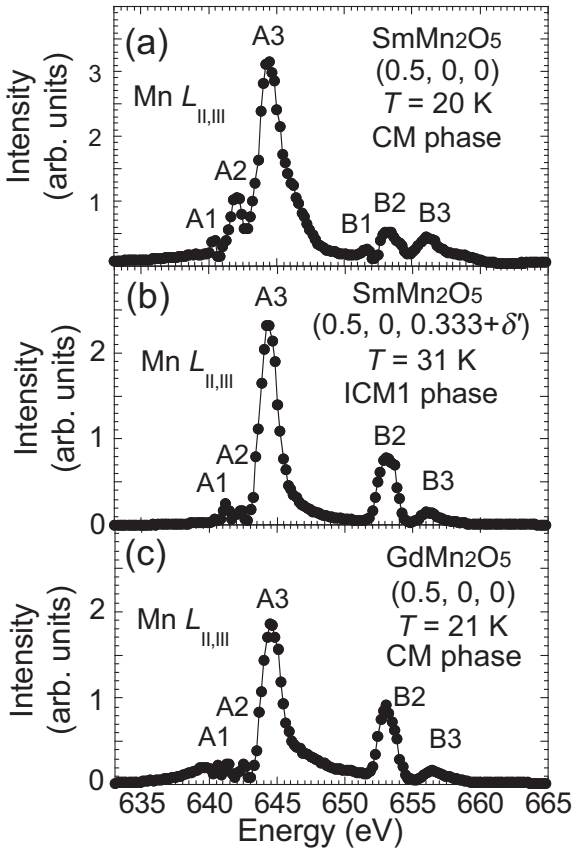

FIG. 3. Energy spectra around Mn $L_{\mathrm{II,III}}$ edges (a) at $\mathbf{Q} = (0.5, 0, 0)$ at $T = 20$ K in the CM phase and (b) at $\mathbf{Q} = (0.5, 0, 0.333+\delta')$ at $T = 31$ K in the ICM1 phase for $SmMn_2O_5$, and (c) at $\mathbf{Q} = (0.5, 0, 0)$ at $T = 20$ K for $GdMn_2O_5$. The incident x-ray was π polarized.

: $\mathbf{q}_{\mathrm{L}} = 2\mathbf{q}_{\mathrm{M}}$ [8,23], which is consistent with the present observation. No resonant peak was observed at Sm M_{IV} edge in this phase, despite careful attempts to acquire this peak. On the basis of these data, we believe that only the long-range ordering of Mn magnetic moments occurs in this phase, and the CM phase with $\mathbf{q}_{\mathrm{M}} = (1/2, 0, 0)$ is triggered by the spontaneous magnetic ordering of Sm ions.

Figures 3(a)–3(b) present the energy spectra around Mn $L_{\mathrm{II,III}}$ edges at $\mathbf{Q} = (0.5, 0, 0)$, $T = 20$ K in the CM phase and at $\mathbf{Q} = (0.5, 0, 0.333+\delta')$, $T = 31$ K in the ICM1 phase, respectively. We also obtained energy spectrum around Mn $L_{\mathrm{II,III}}$ edges at $\mathbf{Q} = (0.5, 0, 0)$ in the CM phase for $GdMn_2O_5$, as shown in Fig. 3(c), for comparison purposes. Recently RHXS measurement at Gd L_{III} edge for $GdMn_2O_5$ has shown that the Gd moments are aligned with $\mathbf{q}_{\mathrm{M}} = (1/2, 0, 0)$ in the CM phase [24]. Our result demonstrates that Mn magnetic moments are also aligned with $\mathbf{q}_{\mathrm{M}} = (1/2, 0, 0)$, which is equivalent to the CM phase in $SmMn_2O_5$. The energy spectrum obtained in $GdMn_2O_5$ is very similar to that acquired in the ICM1 phase of $SmMn_2O_5$. These energy spectra are composed of several peaks, labeled A1 (640.6 eV), A2 (642.1 eV), A3 (644.5 eV), B2 (653.2 eV), and B3 (655.8 eV) in Figs. 3(b), 3(c). In the CM phase of $SmMn_2O_5$, an additional peak labeled B1 (651.6 eV) appears around Mn L_{II} edge, and the intensity of peak A2 increases while that of peak B2 is decreased, as shown in Fig. 3(a). These features were found to be independent of both temperature and azimuthal angle.

In order to investigate the magnetic ordering of oxygen ions, RSXS data were acquired around O K edge in the CM phase. Figures 4(a), 4(b) show energy spectra of resonant scattering at $\mathbf{Q} = (0.5, 0, 0)$ and fluorescence spectra obtained around O K edge in $SmMn_2O_5$ and $GdMn_2O_5$, respectively. The fluorescence background obtained at $\mathbf{Q} = (0.495, 0, 0)$ has been subtracted for each energy spectrum of resonant scattering. The fluorescence background intensities are much weaker than the resonant scattering ones since we used four-blades slit. We observed peak profile around $\mathbf{Q} = (0.5, 0, 0)$ at several energy for $SmMn_2O_5$ and $GdMn_2O_5$, as shown in Figs. 4(c), 4(d), respectively. $GdMn_2O_5$ exhibits main resonant scattering peak in the vicinity of $E = 530$ eV at which point the fluorescence intensity initially increases. A well-defined peak was observed in H scan at $E = 530$ eV, as shown in Fig. 4(d). According to the first-principles calculations of the density of states, this energy range corresponds to the $2p$-$3d$ orbital hybridization between oxygen and Mn ions [25,26]. These results confirm that spin polarization of oxygen ions occurs with $\mathbf{q}_{\mathrm{M}} = (1/2, 0, 0)$ through the $2p$-$3d$ orbital hybridization in $GdMn_2O_5$. Energy spectra similar to that obtained from $GdMn_2O_5$ have been reported for other RMn_2O_5 (R = Tb, Y, Er) and $RMnO_3$ (R = Tb, Dy) compounds [15–18].

In sharp contrast, $SmMn_2O_5$ exhibits no well-defined peak around $E = 530$ eV, as can be seen in Figs. 4(a), 4(c). Although recent RSXS study has shown the possibility that propagation wave vector changes slightly near absorption edge [27], we confirmed the disappearance of the resonant peak for $SmMn_2O_5$ by measuring H $vs.$ E_{photon} intensity map around $\mathbf{Q} = (0.5, 0, 0)$ as shown in Fig. 4(e). Meanwhile nonresonant scattering intensities are apparent below $E = 530$ eV at $T = 20$ K, in the region above which the absorption effect is intensively strong. A well-defined peak also appears in the data from the H scan at $E = 525$ eV, as shown in Fig. 4(c). We also observed the nonresonant scattering even at a different energy such as $E = 1$ keV. Figure 5(a) shows azimuthal dependence of the nonresonant scattering intensity observed at $E = 525$ eV with σ (filled circles) and π (open circles) polarized incident x rays. Using the amplitudes for nonresonant x-ray magnetic scattering [28] and the magnetic structure obtained from neutron scattering analyses [20], we calculated azimuthal dependence of the nonresonant scattering intensity [the solid and dashed lines in Fig. 5(a)]. Since the calculated values reproduced well the azimuthal dependences, it is evident that the nonresonant intensity results from magnetic scattering in $SmMn_2O_5$. The nonresonant intensity disappears at $T = 31$ K ($T > T_{\mathrm{N3}}$ and in the ICM1 phase), as shown in Fig. 4(a). We also observed nonresonant peak for $GdMn_2O_5$ at $E = 525$ eV [shown in Fig. 4(d)], the intensity of which is much lower than that of the resonant scattering peak at $E = 530$ eV. Recent RHXS study for $GdMn_2O_5$ determined that the nonresonant intensity results from magnetic scattering, based on the azimuthal dependence [24].

In addition, several peaks were observed around $E = 535$ eV in $SmMn_2O_5$. One possible explanation for the

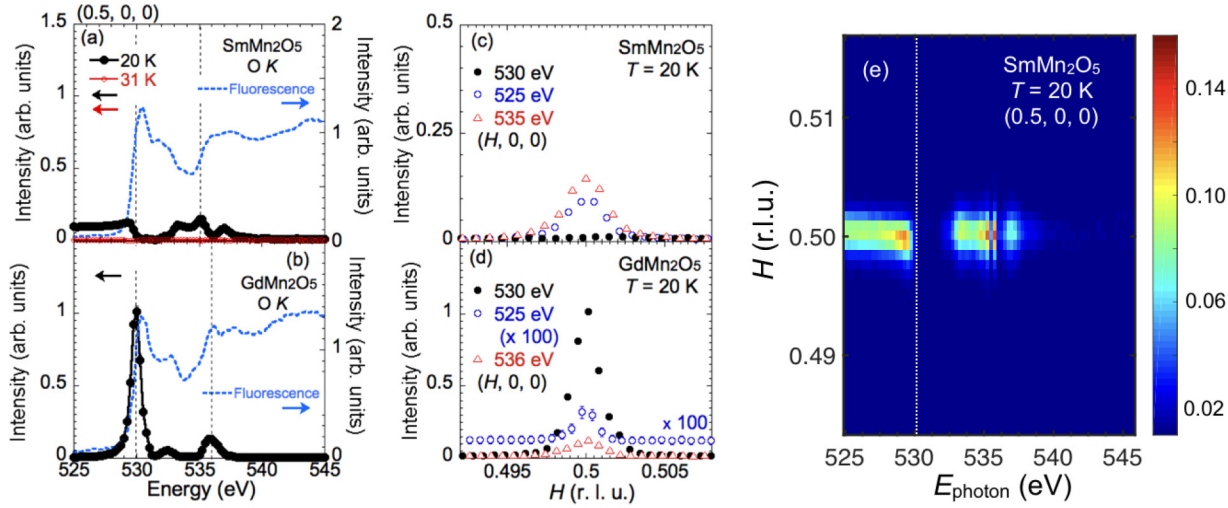

FIG. 4. Energy spectra of Bragg peak intensity at $\mathbf{Q} = (0.5, 0, 0)$ around O K edge (a) at $T = 20$ K (filled circles) and $T = 31$ K (open circles) and the fluorescence spectrum (dashed line) for $SmMn_2O_5$, and (b) $GdMn_2O_5$. The fluorescence background has been subtracted for each energy spectrum of resonant scattering. The H scan peak profile around $\mathbf{Q} = (0.5, 0, 0)$ at each energy for (c) $SmMn_2O_5$ and (d) $GdMn_2O_5$. (e) H *vs*. E_{photon} map of resonant scattering intensity around O K edge at $T = 20$ K for $SmMn_2O_5$. Dashed line indicates $E = 530$ eV. The incident x-ray was π polarized.

appearance of these peaks is nonresonant scattering. Generally, absorption coefficient varies with the incident x-ray energy in the vicinity of an absorption edge. Another possibility is a rare-earth contribution. $GdMn_2O_5$ also exhibited a peak around $E = 536$ eV, as shown in Figs. 4(b), 4(d). This energy range is associated with rare-earth $5d$ states [25,26] and similar rare-earth contributions were also observed in $TbMn_2O_5$ and $RMnO_3$ (R = Tb, Dy) [17,18]. Furthermore, the intensity around $E = 535$ eV in $SmMn_2O_5$ is comparable to that of the nonresonant scattering, in spite of a strong absorption effect. Therefore, these intensities might result from both nonresonant and resonant magnetic scattering. Figure 5(b) shows azimuthal dependence of the intensity at $E = 535$ eV. The solid and dashed lines represent the calculated azimuthal dependence of the intensities with σ and π polarized incident x-rays, respectively, assuming that the intensity at $E = 535$ eV is due to resonant magnetic scattering and that the magnetic moments of oxygen ions have only a c axis component. Although these calculations reproduce the experimental values quite well, the exact origin of these peaks is presently unclear, since the nonresonant scattering exhibits a similar azimuthal dependence in Fig. 5(a). A polarization analysis for scattered x ray would be required to determine this.

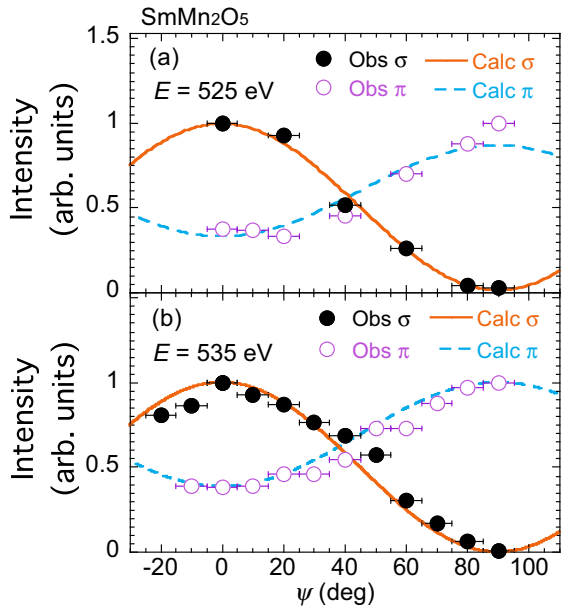

FIG. 5. Azimuthal dependence of (a) the nonresonant scattering observed at $E = 525$ eV and (b) the intensity at $E = 535$ eV in the CM phase for $SmMn_2O_5$ with σ (filled circles) and π (open circles) polarized incident x rays. The solid and dashed lines in both figures represent the calculated values for the σ and π polarized incident x rays, respectively. By definition, azimuthal angle of $\psi = 90^\circ$ indicates that the c^* axis is perpendicular to the scattering plane.

It is typically difficult to compare the RSXS intensities acquired from different samples because of the strong effect of the sample surface conditions on the scattering intensity. However, it is possible to compare the energy spectra in Figs. 4(a), 4(b) since both were normalized relative to the calculated nonresonant magnetic scattering values at $E = 525$ eV, using the magnetic structures of $SmMn_2O_5$ and $GdMn_2O_5$ [20,29].

Figure 6(a) shows temperature dependence of scattering intensities at Sm M_{IV} and Mn L_{III} edges, as well as the lattice modulation. Below T_{CM}, the $\mathbf{Q} = (0.5, 0, 0)$ scattering intensities increase at both the Sm M_{IV} and Mn L_{III} edges. Scattering intensity at $\mathbf{Q} = (0.5, 0, 0.333+\delta')$ at Mn L_{III} edge appears at $T_{\text{N2}} \simeq 34$ K and disappears at $T_{\text{CM}} \simeq 26$ K. In addition, lattice modulation with $\mathbf{q}_{\text{L}} = (0, 0, 2/3 + 2\delta')$ is observed between T_{N2} and $T_{\text{N3}} \simeq 28$ K. There is simultaneous magnetic ordering of Sm and Mn ions with $\mathbf{q}_{\text{M}} = (1/2+\delta, 0, 0)$ and of Mn ions with $\mathbf{q}_{\text{M}} = (1/2, 0, 1/3+\delta')$ between T_{N3} and T_{CM}. As shown in Fig. 6(b), intensity at $E = 535$ eV appears below T_{N3} at the reciprocal lattice point $Q = (0.5+\delta, 0, 0)$ which changes to the $Q = (0.5, 0, 0)$ at T_{CM}. The $(0.5, 0, 0.333+\delta')$ reflections in the ICM1 and ICM2 phases cannot

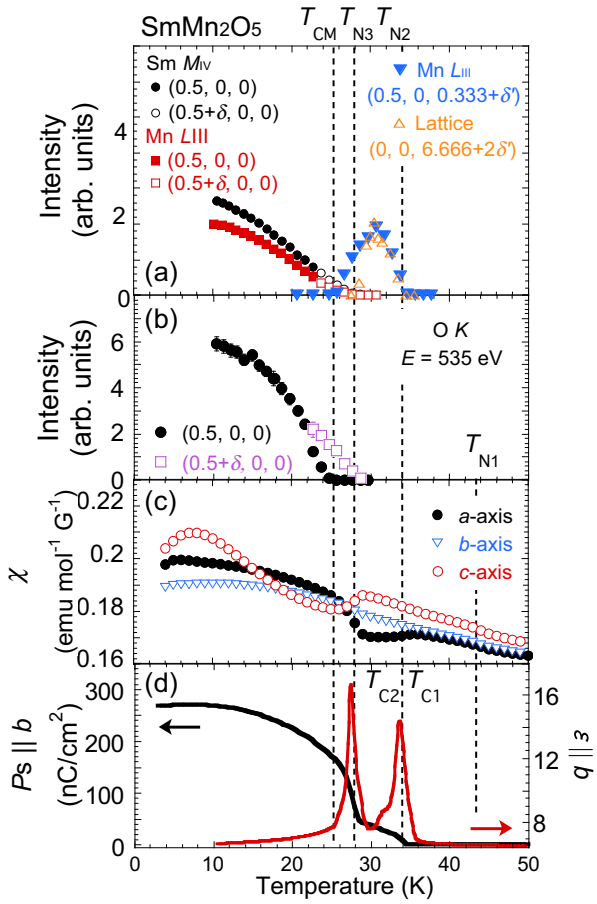

FIG. 6. Temperature dependence of the scattering intensities (a) at Sm M_{IV}, Mn L_{III} edges and lattice modulation, and (b) at O K edge. Temperature dependence of (c) the magnetic susceptibility and (d) the dielectric constant (red line) and the electric polarization (black line) along the b axis. (c) and (d) are taken from Ref. [19].

be observed around O K edge by RSXS measurement because of the limitation of Q range.

Figures 6(c) and 6(d) show temperature dependence of the magnetic susceptibilities along the each crystallographic axis, and dielectric constant and electric polarization along the b axis, respectively [19]. These measurements confirm that ferroelectric transitions occur simultaneously with antiferromagnetic transitions.

IV. DISCUSSION

The incommensurate ordering of the Mn magnetic moments occurs with $\mathbf{q}_M = (1/2, 0, 1/3+\delta')$ between T_{N2} and T_{CM}, which is similar to the magnetic ordering observed in $EuMn_2O_5$ [30]. We confirmed the appearance of ICM1 phase as shown in Fig. 1, which coexists with FE1 phase. Lattice modulation with $\mathbf{q}_M = (0, 0, 2/3 + 2\delta')$ also occurs in this phase, which indicates that local electric polarizations align in a compensated structure along the c axis, i.e., no net component. That results in a relatively weak electric polarization in the FE1 (ICM1) phase. Conversely, lattice modulation occurs with in-phase along the c axis in the FE2 (ICM2 and CM) phase, which gives rise to a large electric polarization, as has been discussed in our previous report [19]. Between T_{N3} and T_{CM}, ICM1 and ICM2 phases coexist, as can be seen in Fig. 1.

The energy spectrum around Mn $L_{II,III}$ edges in the ICM1 phase of $SmMn_2O_5$ is quite similar to that obtained in the CM phase of $GdMn_2O_5$ [see Figs. 3(b), 3(c)]. Other RMn_2O_5 (R = Tb, Er, Y) compounds also exhibit similar energy spectra around Mn $L_{II,III}$ edges [16,31,32]. However, the energy spectrum in the CM phase of $SmMn_2O_5$ is different from those in the ICM1 phase of $SmMn_2O_5$ and in other RMn_2O_5 materials. Previous RSXS studies for RMn_2O_5 (R = Tb, Er, Y) compounds have found that the shape of the energy spectra is modified by variations in both temperature and azimuthal angle. This effect has been attributed to the different contributions of Mn^{4+} and Mn^{3+} ions to the magnetic structure factor due to the formation of complex noncollinear magnetic structures.

However, the shape of the energy spectrum in the CM phase of $SmMn_2O_5$ shows neither temperature nor azimuthal angle dependence. Furthermore, both $SmMn_2O_5$ and $GdMn_2O_5$ have almost collinear magnetic structures in the CM phase. The Mn^{4+} and Mn^{3+} magnetic moments form equivalent spin arrangements such as zigzag antiferromagnetic chains in the ab plane in both materials, although the moments point to the c axis in $SmMn_2O_5$ and the a axis in $GdMn_2O_5$ [19,20,29]. Thus the different energy spectra in the CM phase of $SmMn_2O_5$ likely reflect the unique electronic state of Mn ions in the CM phase of $SmMn_2O_5$ rather than the different magnetic structure of the Mn ions.

It has recently been reported that oxygen spin polarization is primarily induced by $2p$-$3d$ hybridization between oxygen and Mn ions in RMn_2O_5 (R = Tb, Y, Er) and $RMnO_3$ (R = Tb, Dy) materials [15–18]. $GdMn_2O_5$ also exhibited a well-defined peak around E = 530 eV [see Figs. 4(b), 4(d)], where fluorescence exhibited first edge, which corresponds to the $2p$-$3d$ hybridization [25,26]. A recent RSXS study of oxygen spin polarization in YMn_2O_5 has suggested that $\mathbf{P}_{ele}$ resulting from p-d hybridization between oxygen and Mn ions plays a key role for the ferroelectricity [15]. The energy spectrum around O K edge in $SmMn_2O_5$ is quite different from those in other RMn_2O_5 materials, in which there is no well-defined peak in the vicinity of E = 530 eV. Our previous RHXS [19] and recent neutron scattering experiments [20] identified an almost collinear magnetic structure in the CM phase in $SmMn_2O_5$, whereas Mn moments align in a noncollinear manner along the c axis in other RMn_2O_5 compounds [4,33,34]. This result suggests that exchange striction is primarily responsible for the ferroelectricity in $SmMn_2O_5$. Our present work also provides strong evidence that $\mathbf{P}_{ele}$ does not significantly contribute to the large electric polarization in this material, which is probably cased by $\mathbf{P}_{ion}$ dominantly in the collinear magnetic structure of $SmMn_2O_5$.

Mn magnetic moments point to the c axis in $SmMn_2O_5$ and the a axis dominantly in the other RMn_2O_5 compounds [4,19,20,29,33,34]. This difference maybe causes the disappearance of oxygen spin polarization resulting from p-d hybridization and $\mathbf{P}_{ele}$ in the CM phase of $SmMn_2O_5$ due to exchange interaction between Mn and oxygen spin. The disappearance of $\mathbf{P}_{ele}$ likely changes the effective charges of Mn^{3+} and Mn^{4+} ions [12] from those in the ICM1 phase,

which could change the shape of an energy spectrum of resonant scattering around Mn $L_{II,III}$ edges, although the fluorescence spectrum remain almost unchanged in the CM phase of $SmMn_2O_5$. On the other hand, some theoretical studies of manganese oxides have shown that crystal field effect can modify the shape of an energy spectrum around Mn $L_{II,III}$ edges [35–37]. The different energy spectrum around Mn $L_{II,III}$ edges in the CM phase is possibly caused by changes the environment around the Mn sites due to the lattice distortion. Therefore further theoretical studies and structural analysis would be required to confirm them.

V. SUMMARY

RSXS was used to investigate the magnetic ordering in multiferroic compounds $SmMn_2O_5$ and $GdMn_2O_5$. In the case of $SmMn_2O_5$, we confirmed the existence of an ICM1 phase in which only the Mn magnetic moments are ordered with $\mathbf{q}_M = (1/2, 0, 1/3+\delta)$. The energy spectrum around Mn $L_{II,III}$ edges in the CM phase in $SmMn_2O_5$ is different from those acquired in the ICM1 phase and in $GdMn_2O_5$, probably due to the unique electronic state of the Mn ions in the CM phase of $SmMn_2O_5$. The energy spectrum around O K edge suggests that $\mathbf{P}_{ele}$ makes only a minor contribution to the large electric polarization in the collinear magnetic structure of $SmMn_2O_5$.

ACKNOWLEDGMENTS

We greatly acknowledge F. Oba, Y. Kumagai, and N. Tsunoda for calculating DOS of $SmMn_2O_5$ and $GdMn_2O_5$. This study was supported by KAKENHI program for Scientific Research (A) (JP15H02038, JP17K05130) and (B) (24340064), Challenging Exploratory Research (2365409), Dynamic Alliance for Open Innovation Bridging Human, Environment and Materials, and a KEK-IMSS grant for Quantum Beam Research. This work was performed with the approval of the Photon Factory Program Advisory Committee (Proposals No. 2012S2-005, No. 2013G045, No. 2013G071, No. 2015G029, No. 2016PF-BL-19B, No. 2017G018, and No. 2017G549).

[1] D. Khomskii, Physics **2**, 20 (2009).
[2] N. Hur, S. Park, P. A. Sharma, J. S. Ahn, S. Guha, and S.-W. Cheong, Nature (London) **429**, 55 (2004).
[3] M. Fukunaga, Y. Sakamoto, H. Kimura, Y. Noda, N. Abe, K. Taniguchi, T. Arima, S. Wakimoto, M. Takeda, K. Kakurai, and K. Kohn, Phys. Rev. Lett. **103**, 077204 (2009).
[4] C. Vecchini, L. C. Chapon, P. J. Brown, T. Chatterji, S. Park, S.-W. Cheong, and P. G. Radaelli, Phys. Rev. B **77**, 134434 (2008).
[5] J.-H. Kim, S.-H. Lee, S. I. Park, M. Kenzelmann, A. B. Harris, J. Schefer, J.-H. Chung, C. F. Majkrzak, M. Takeda, S. Wakimoto, S. Y. Park, S.-W. Cheong, M. Matsuda, H. Kimura, Y. Noda, and K. Kakurai, Phys. Rev. B **78**, 245115 (2008).
[6] D.-J. Huang, J. Okamoto, S.-W. Huang, and C.-Y. Mou, J. Phys. Soc. Jpn. **79**, 011009 (2010).
[7] S. Wakimoto, H. Kimura, Y. Sakamoto, M. Fukunaga, Y. Noda, M. Takeda, and K. Kakurai, Phys. Rev. B **88**, 140403(R) (2013).
[8] Y. Noda, H. Kimura, M. Fukunaga, S. Kobayashi, I. Kagomiya, and K. Kohn, J. Phys.: Condens. Matter **20**, 434206 (2008).
[9] W. Ratcliff, II, V. Kiryukhin, M. Kenzelmann, S.-H. Lee, R. Erwin, J. Schefer, N. Hur, S. Park, and S. W. Cheong, Phys. Rev. B **72**, 060407(R) (2005).
[10] H. Kimura, Y. Kamada, Y. Noda, K. Kaneko, N. Metoki, and K. Kohn, J. Phys. Soc. Jpn. **75**, 113701 (2006).
[11] H. Kimura, S. Wakimoto, M. Fukunaga, Y. Noda, K. Kaneko, N. Metoki, K. Kakurai, and K. Kohn, J. Phys. Soc. Jpn. **78**, 034718 (2009).
[12] G. Giovannetti and J. van den Brink, Phys. Rev. Lett. **100**, 227603 (2008).
[13] A. S. Moskvin and R. V. Pisarev, Phys. Rev. B **77**, 060102(R) (2008).
[14] T.-R. Chang, H.-T. Jeng, C.-Y. Ren, and C.-S. Hsue, Phys. Rev. B **84**, 024421 (2011).
[15] S. Partzsch, S. B. Wilkins, J. P. Hill, E. Schierle, E. Weschke, D. Souptel, B. Büchner, and J. Geck, Phys. Rev. Lett. **107**, 057201 (2011).
[16] R. A. de Souza, U. Staub, V. Scagnoli, M. Garganourakis, Y. Bodenthin, S.-W. Huang, M. García-Fernández, S. Ji, S.-H. Lee, S. Park, and S.-W. Cheong, Phys. Rev. B **84**, 104416 (2011).
[17] T. A. W. Beale, S. B. Wilkins, R. D. Johonson, D. Prabhakaran, A. T. Boothroyd, P. Steadman, S. S. Dhesi, and P. D. Hatton, Eur. Phys. J. Special Topics **208**, 99 (2012).
[18] S. W. Huang, J. M. Lee, H.-T. Jeng, YuCheng Shao, L. Andrew Wray, J. M. Chen, R. Qiao, W. L. Yang, Y. Cao, J.-Y. Lin, R. W. Schoenlein, and Y.-D. Chuang, Phys. Rev. B **94**, 035145 (2016).
[19] Y. Ishii, S. Horio, M. Mitarashi, T. Sakakura, M. Fukunaga, Y. Noda, T. Honda, H. Nakao, Y. Murakami, and H. Kimura, Phys. Rev. B **93**, 064415 (2016).
[20] G. Yahia, F. Damay, S. Chattopadhyay, V. Balédent, W. Peng, E. Elkaim, M. Whitaker, M. Greenblatt, M.-B. Lepetit, and P. Foury-Leylekian, Phys. Rev. B **95**, 184112 (2017).
[21] B. M. Wankly, J. Mater. Sci. **7**, 813 (1972).
[22] H. Nakano, Y. Yamasaki, J. Okamoto, T. Sudayama, Y. Takahashi, K. Kobayashi, R. Kumai, and Y. Murakami, J. Phys.: Conf. Ser. **502**, 012015 (2014).
[23] Y. Noda, H. Kimura, Y. Kamada, Y. Ishikawa, S. Kobayashi, Y. Wakabayashi, H. Sawa, N. Ikeda, and K. Kohn, J. Korean Phys. Soc. **51**, 828 (2007).
[24] N. Lee, C. Vecchini, Y. J. Choi, L. C. Chapon, A. Bombardi, P. G. Radaelli, and S.-W. Cheong, Phys. Rev. Lett. **110**, 137203 (2013).
[25] F. El Hallani, S. Naji, H. Ez-Zahraouy, and A. Benyoussef, J. Appl. Phys. **114**, 163909 (2013).
[26] M. Ait Tamerd, B. Abraime, A. Abbassi, K. El Maalam, A. El Kenz, A. Benyoussef, M. Balli, M. Hamedoun, and O. Mounkachi, J. Phys: Conf. Ser. **758**, 012009 (2016).
[27] H. Jang, B. Y. Kang, B. K. Cho, M. Hashimoto, D. Lu, C. A. Burns, C.-C. Kao, and J.-S. Lee, Phys. Rev. Lett. **117**, 216404 (2016).

[28] J. P. Hill and D. F. McMorrow, Acta Crystallogr. Sect. A **52**, 236 (1996).

[29] G. Yahia, F. Damay, S. Chattopadhyay, V. Balédent, W. Peng, S. W. Kim, M. Greenblatt, M.-B. Lepetit, and P. Foury-Leylekian, Phys. Rev. B **97**, 085128 (2018).

[30] V. Polyakov, V. Plakhty, M. Bonnet, P. Burlet, L.-P. Regnault, S. Gavrilov, I. Zobkalo, and O. Smirnov, Physica B (Amsterdam) **297**, 208 (2001).

[31] U. Staub, Y. Bodenthin, M. García-Fernández, R. A. de Souza, M. Garganourakis, E. I. Golovenchits, V. A. Sanina, and S. G. Lushnikov, Phys. Rev. B **81**, 144401 (2010).

[32] J. Koo, C. Song, S. Ji, J.-S. Lee, J. Park, T.-H. Jang, C.-H. Yang, J.-H. Park, Y. H. Jeong, K.-B. Lee, T. Y. Koo, Y. J. Park, J.-Y. Kim, D. Wermeille, A. I. Goldman, G. Srajer, S. Park, and S.-W. Cheong, Phys. Rev. Lett. **99**, 197601 (2007).

[33] H. Kimura, S. Kobayashi, Y. Fukuda, T. Osawa, Y. Kamada, Y. Noda, I. Kagomiya, and K. Kohn, J. Phys. Soc. Jpn. **76**, 074706 (2007).

[34] G. R. Blake, L. C. Chapon, P. G. Radaelli, S. Park, N. Hur, S.-W. Cheong, and J. Rodríguez-Carvajal, Phys. Rev. B **71**, 214402 (2005).

[35] C. W. M. Castleton and M. Altarelli, Phys. Rev. B **62**, 1033 (2000).

[36] S. B. Wilkins, P. D. Spencer, P. D. Hatton, S. P. Collins, M. D. Roper, D. Prabhakaran, and A. T. Boothroyd, Phys. Rev. Lett. **91**, 167205 (2003).

[37] K. J. Thomas, J. P. Hill, S. Grenier, Y.-J. Kim, P. Abbamonte, L. Venema, A. Rusydi, Y. Tomioka, Y. Tokura, D. F. McMorrow, G. Sawatzky, and M. van Veenendaal, Phys. Rev. Lett. **92**, 237204 (2004).